ACS APPLIED MATERIALS & INTERFACES

www.acsami.org

Research Article

Ultrathin Stretchable Triboelectric Nanogenerators Improved by Postcharging Electrode Material

Weiyi Zhang, Qiang Liu, Shengyu Chao, Ruping Liu, Xi Cui, Yu Sun, Han Ouyang,* and Zhou Li*

Cite This: *ACS Appl. Mater. Interfaces* 2021, 13, 42966–42976

Read Online

ACCESS | Metrics & More | Article Recommendations | Supporting Information

ABSTRACT: Sustainable ultrathin stretchable power sources have emerged with the development of wearable electronics. They obtain energy from living organisms and the environment to drive these wearable electronics. Here, an ultrathin stretchable and triboelectric nanogenerator (TENG) improved by chargeable carbon black (CB)/thermoplastic polyurethane (TPU) composite material (CT-TENG) is proposed for mechanical energy harvesting and physiological signal sensing. The CB/TPU composite can act as both a stretchable electrode and a triboelectric layer due to the coexistence of conductive CB and dielectric TPU. The CT-TENG demonstrates good stretchability (≈646%), ultrathin thickness (≈50 μm), and a lightweight (≈62 mg). The triboelectric electrode material can be improved by postcharging treatment. With the corona charging process, the output performance of the CT-TENG was improved eightfold and reached 41 V. Moreover, the CT-TENG with a self-powered sensing capability can inspect the amplitude and frequency of different physiological movements. Consequently, the CT-TENG is promising in promoting the development of electronic skins, wearable systems of self-powered sensors, human−machine interactions, soft robotics, and artificial intelligence applications.

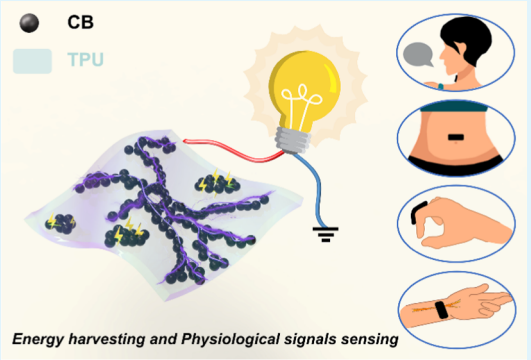

KEYWORDS: *postcharging treatment, energy harvesting, self-powered, physiological signal sensing, triboelectric nanogenerators*

INTRODUCTION

Rapid progress in the Internet-of-Things and artificial intelligence has significantly promoted intelligent wearable electronic devices.[1−4] Among all sorts of wearable/portable electronics, sensors with high stretchability have attracted intensive research in human motion sensing, personal healthcare monitoring, soft robotics, and human−machine interfaces.[5−8] However, a sustainable and reliable power supply is usually required for most of these devices, which restricts the applicability and lifespan of wearable electronics.[9−12] Moreover, a proper power source also needs to meet the demands of low cost, large-scale production, biocompatibility, and flexibility or stretchability.[13−15] Therefore, it is urgently needed but still challenging to develop energy devices that satisfy the abovementioned requirements while harvesting mechanical energy to directly power wearable electronics.[16−19]

Triboelectric nanogenerators (TENGs) have been developed to convert the extensively existing low-frequency and irregular mechanical energy from ambient environments into electrical energy.[20−25] Its working principle is based on the triboelectric effect and electrostatic induction. Because of its many material selections, TENGs could be a promising choice for dependable self-sustainable energy harvesters and self-powered sensors.[26−28] Among the stretchable TENGs presented previously, single-electrode TENGs are more promising owing to their relatively simple, thin structure and convenience for carrying.[29] Currently, most stretchable single-electrode TENGs are fabricated from conductive flexible materials, including conductive composites,[30,31] ionic liquids/hydrogels,[32,33] and knitted conductive fibers/yarns.[2,34] Nevertheless, the thickness of the electrodes cannot usually reach the ultrathin level, and thus the reported samples to date are too thick.[16]

Most stretchable TENGs remain thick, limiting the comfort and compatibility of the device. Although some ionic hydrogels possess excellent stretchability, dehydration occurs or the liquid solvent will evaporate. As a result, their stability cannot be maintained over a long period of time, together with poor mechanical strength and low conductivity, restricting their applications in practice. Moreover, the fabrication of conductive fibers contains many complex procedures that inevitably constrain the broad use in energy harvesters and sensors. Conductive composites as stretchable electrodes with good conductivity, flexibility, stretchability, and large-scale production have been intensively investigated for self-powered

Received: July 21, 2021
Accepted: August 23, 2021
Published: September 2, 2021

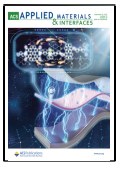

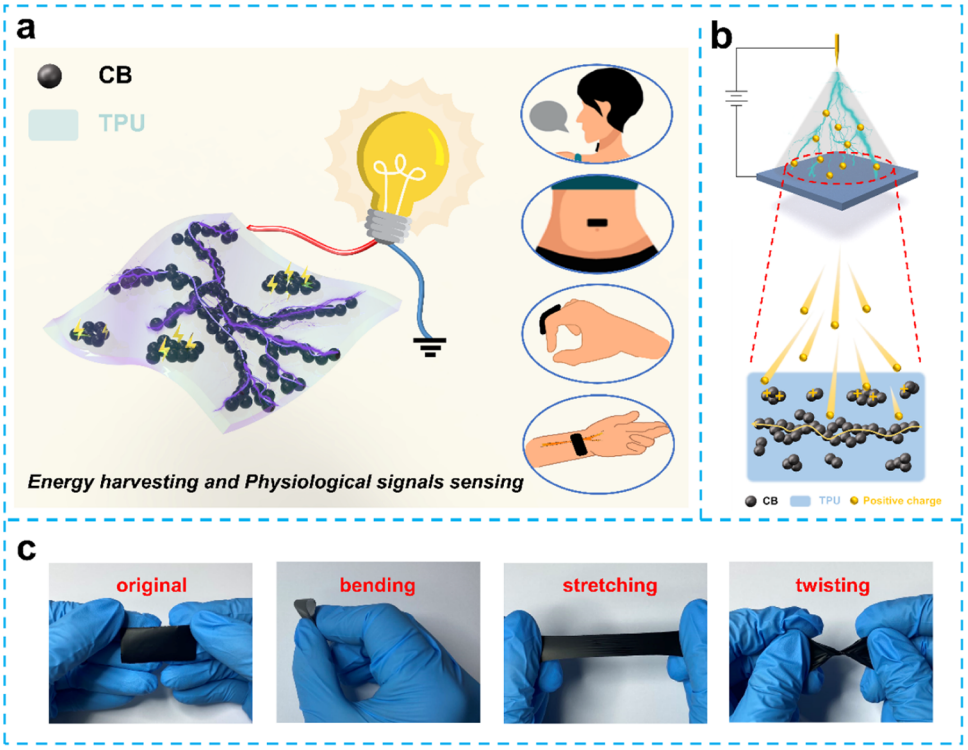

Figure 1. (a) Schematic illustration showing the detailed inner structure of the single-electrode CT-TENG. (b) Schematic illustration of the corona charging process. (c) Photographs of the CT-TENG in the original, bending, stretching, and twisting states.

sensors. Various conductive fillers, including silver nanowires,[35] carbon black (CB),[30] carbon nanotubes (CNTs),[31] graphene,[36] liquid metal,[37] and conductive polymers,[38] are embedded into the elastomer matrix as stretchable electrodes.

CB has been considered a proper filler owing to its high conductivity, easy availability, low cost, and low specific weight,[38] while the charge storage ability of CB particles has been demonstrated in the literature, and the charge storage ability of the TENG contact layer can remarkably improve due to the presence of CB.[39] On the other hand, flexible elastomers are widely used as flexible materials for stretchable TENGs because of their high elongation at breakpoint (strain > 100%), such as poly(dimethylsiloxane) (PDMS), thermoplastic polyurethane (TPU), and Ecoflex. TPU was selected as the matrix in this study due to its good mechanical strength, excellent elasticity, flexibility, and facile melt processability compared with other elastomers/rubbers.[40]

In addition, their limited electrical output performance also impedes the further development of conductive composite-based TENGs. Although corona charging treatment for performance improvement has been studied in previous reports,[41,42] conductive composite-based electrodes of TENGs treated with this method have rarely been discussed. To address these issues, a strategy for improving the output performance of a stretchable and ultrathin conductive composite-based single-electrode TENG is required.

Herein, we demonstrate a simple, large-scale, and low-cost fabrication process for an ultrathin and stretchable single-electrode TENG (CT-TENG) based on a chargeable CB/TPU composite. After corona charging, the developed CT-TENG can reach an open-circuit voltage (V_{OC}) of ≈ 41 V, which is 8 times higher than that of the pristine CT-TENG, a short-circuit current (I_{SC}) of ≈ 0.262 μA and a short-circuit transferred charge (Q_{SC}) of ≈ 14 nC, compared with ≈ 0.082 μA and ≈ 3 nC of the pristine device, respectively. The CT-TENG can power commercial electronics by harvesting mechanical energy without external power supply. Furthermore, the CT-TENG can also be utilized as a self-powered sensor to detect physiological signals when attached to different parts of the human body. The proposed stretchable and ultrathin CT-TENG improved by the CB/TPU composite demonstrates excellent potential for development in energy harvesting, self-powered wearable electronics, and biomedical sensors.

RESULTS AND DISCUSSION

Fabrication of the CT-TENG and Its Characterization.

Figure 1a illustrates the CT-TENG, which is working in a single-electrode mode. CB percolated networks and charged CB particles embedded in the TPU matrix construct the internal structure of the CT-TENG. It can be clearly seen that the CBs are distributed evenly throughout the TPU. Several conductive paths are formed and connected for current flow, while some individual islands made of aggregated CBs are also formed. TPU possesses good mechanical strength, elasticity, flexibility, and facile melt processability; CB is also conductive, has low cost, and is readily available. Taking advantage of both TPU and CB, the as-obtained conductive CB/TPU composite can be regarded as a stretchable electrode and a triboelectrification layer. Hence, the CT-TENG can work stably under stretching. Because the pure TPU is electrically insulated and there are no connections among those individual islands and conductive networks, the current will not pass through the islands. Generally, varying the content of CB in a flexible elastomer can influence the electrical characteristics of the composite.[38,40,43] When the filling content of CB is low, the CBs are mainly in the form of isolated islands, showing almost insulated properties. With increasing CB content, percolated

https://doi.org/10.1021/acsami.1c13840
ACS Appl. Mater. Interfaces 2021, 13, 42966−42976

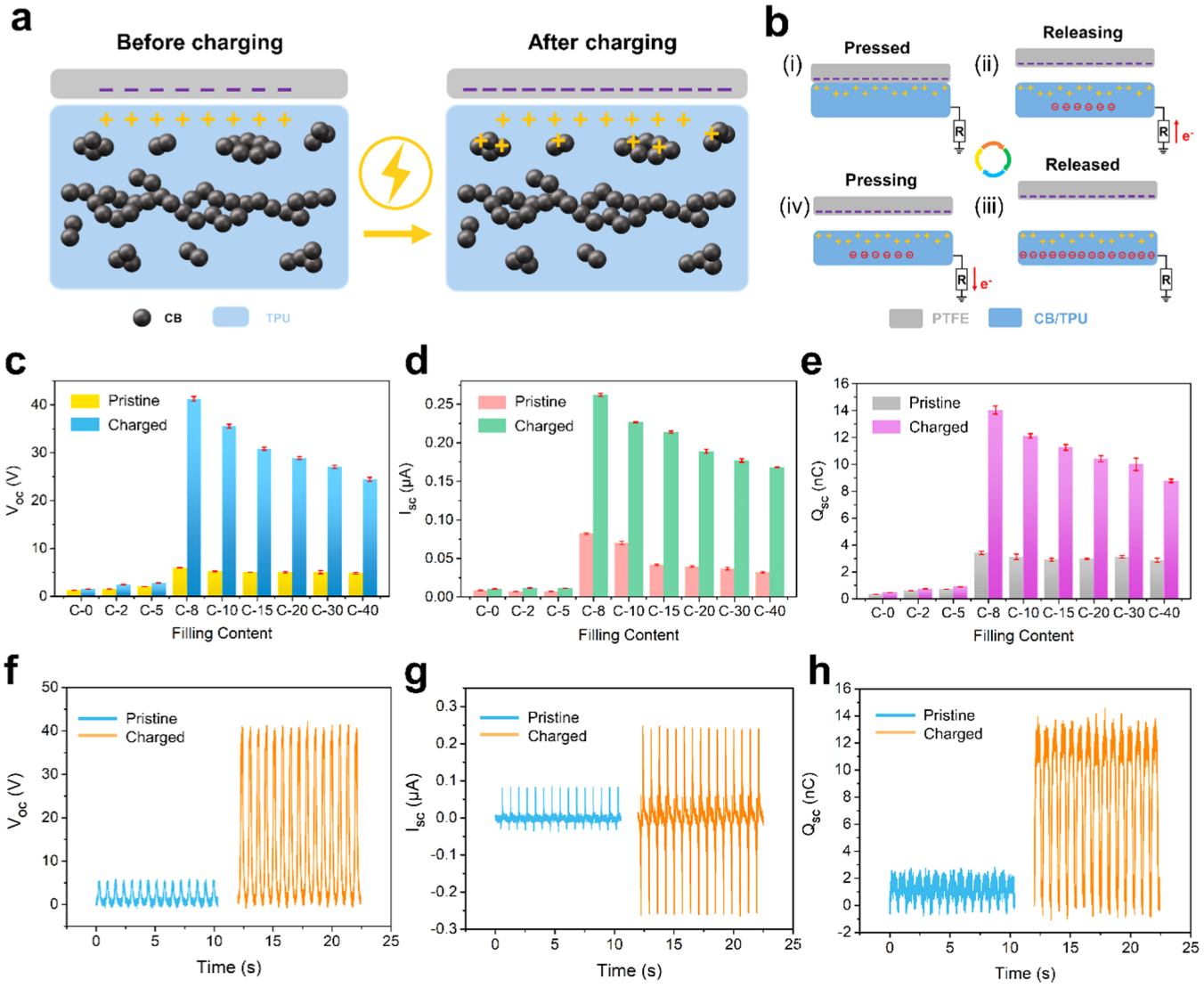

Figure 2. Working mechanism and output performance of the CT-TENG in single-electrode mode. (a) Schematic diagram of the charge distribution of the CT-TENG caused by the contact triboelectrification effect before and after corona charging. (b) Schematics of the operating principle for the CT-TENG. (c–e) Comparison of V_{OC}, I_{SC}, and Q_{SC} of the CT-TENG with different CB filling contents before and after corona charging. (f–h) Comparison of V_{OC}, I_{SC}, and Q_{SC} of C-8 before and after corona charging.

conductive networks form but isolated islands still exist. As a result, the conductivity extremely increases by several orders of magnitude. The ascending trend of the conductivity change will be gentle under a relatively saturated concentration range. Thus, a denser, interlinked network of CBs is constructed in the TPU.

In this work, we chose CB/TPU composites with various CB contents (2, 5, 8, 10, 15, 20, 30, and 40%) as the CT-TENG. For comparison, a TENG based on pure TPU was also fabricated. For convenience, the CT-TENGs made of different CB mass ratios are denoted as C-0, C-2, C-5, C-8, C-10, C-15, C-20, C-30, and C-40. The surface morphology of these samples is shown in Figure S1, indicating a homogeneous composite of CB and TPU. Moreover, the conductivity change of these samples is in accord with a typical percolation transition behavior, as shown in Figure S2. This result is also consistent with a previous report,[40] indicating that an increasing number of conductive paths are formed with increasing CB content in the TPU. The CB content cannot exceed 40% to maintain the flexible properties of the TPU for the CT-TENG.

To demonstrate the flexibility, various states of the CT-TENG like bending, stretching, and twisting are shown in Figure 1c. Additionally, because of the low cost of the raw materials, equipment accessibility, and a simple fabrication process, it is feasible to achieve large-scale fabrication of the CB/TPU composite. As illustrated in Figure S3, a film made of a C-8 composite with dimensions of 30 × 30 cm^2 was successfully fabricated, showing the potential for large-scale fabrication in real applications. The size of the film can be further tuned by changing the dimension of the mold. In addition, the device is very thin and lightweight, only 50 μm and 62 mg (area, 2 × 4 cm^2), respectively, as shown in Figure S4a,b.

Fourier transform infrared (FT-IR) spectra of the CB/TPU composites with different CB contents were recorded to investigate the interaction between CB and TPU. As shown in Figure S5a, the stretching vibrations of the N–H bonds located at approximately 3324 cm^{-1} in polyurethane were

https://doi.org/10.1021/acsami.1c13840
ACS Appl. Mater. Interfaces 2021, 13, 42966–42976

highly sensitive to hydrogen bonding. The peak shift verifies that H-bonding interactions exist between the N−H groups of TPU and the remaining oxygenated groups of CB, indicating an interaction between TPU and CB. The peaks at 2955 and 2870 cm^{-1} were assigned to alkene−CH stretching vibrations. Moreover, the two characteristic peaks at 1730 and 1700 cm^{-1} shown in Figure S5b, which were attributed to free C═O and H-bonded C═O, were used to confirm the presence of hydrogen bonding between CB and TPU. CB contains −OH, C═O, and −COOH groups, which easily form hydrogen bonds with the urethane and ester groups of TPU.[44] With the addition of CB, the peak intensity of these characteristic peaks becomes weaker, which could be attributed to the fact that aggregated CB particles hinder the formation of extra hydrogen bonds at a higher filling content.

To improve the output performance of the CT-TENG, corona charging was conducted to charge the device with more positive charges. During this process, the corona needle tip was connected to the positive end of a polarization voltage source, and the CT-TENG was connected to the other end through the lead wire. Under a high polarization voltage, the isolated CB islands made of embedded CB nanoparticles in the TPU matrix acted as charge-trapping sites, which increased the active interface for charge storage. Positive charges attracted from the CB through the corona charging process were stored either in the discrete CB nanoparticles or trapped in the isolated CB islands. Both might result in a high surface charge density on the CB/TPU composite and a low dissipation rate of surface charge. A schematic diagram of the detailed corona charging processes for the CT-TENG is depicted in Figures 1b and S6.

Working Mechanism. The working mechanism of the CT-TENG is based on the coupling effect of tribo-electrification and electrostatic induction, which is shown in Figure 2a,b. Since poly(tetrafluoroethylene) (PTFE) is an electronegative polymer material with strong electron-accepting capability, the PTFE film acts as a negative triboelectric material, and thus TPU is a positive triboelectric material. As shown in Figure 2a, after corona charging, the charges stored in the CB islands enhance the triboelectrification effect of the CT-TENG. The CT-TENG is connected to the ground by a lead wire, working in a single-electrode mode. When an active object is in full contact with the CT-TENG surface, the electrification process occurs at its interface. The generated triboelectric charges with opposite polarities are fully balanced, so no electrons flow in the external circuit. Here, a PTFE film was used as the moving object. Additionally, inside the CT-TENG, the conductive networks made of CB can be regarded as the electrode.

For the charged CT-TENG, the amount of the generated triboelectric charges are obviously increased under the full contact state, as displayed in Figure 2b. When the PTFE film starts to separate from the CT-TENG surface, the potential difference increases and the contact-induced triboelectric charges cannot be equilibrated. Consequently, negative charges are induced in the conductive CB networks to reach an electrical equilibrium state, resulting in instantaneous electron flow through the external load from the ground to the electrode, so an electrical output signal can be detected. When the two contacting surfaces are completely separated, the positive charges of the CT-TENG are fully insulated from the induced negative charges in the conductive CB networks. As the PTFE film approaches the CT-TENG again, the electrons flow back to the ground from the conductive CB networks, forming a reverse output signal. After complete contact of the PTFE film with the CT-TENG, the system returns to the original state again. Therefore, an alternating current can be obtained by repeated contact and separation cycles. As shown in Figure S7, the corresponding simulation using COMSOL software was also conducted to simulate the potential distributions under different states of CT-TENG and verify the working mechanism.

Electrical Output Performance. To evaluate the electrical output performance of the CT-TENG, a commercial PTFE film was employed as a moving object and a mechanical linear motor was used to provide periodic contact-separation motion. The contact area was chosen as 2 × 4 cm^2, and the maximum movement distance was set as 3 cm. To analyze how the CB mass ratio of the CB/TPU composite impacts the output performance of the CT-TENG before and after corona charging treatment, several samples with different CB mass ratios were fabricated. It can be clearly seen that for both the pristine and charged samples, the output performance of V_{OC}, I_{SC}, and Q_{SC} increases gently at first, then it increases sharply at C-8, and subsequently keeps declining with increasing CB mass ratio (Figures 2c−e and S8).

For C-0, C-2, and C-5, their V_{OC}, I_{SC}, and Q_{SC} are far less than those of other samples before and after corona charging. This could be ascribed to the insulated property of these low filling level samples. In these cases, they can only be regarded as the dielectric triboelectrification layer without the electrode, so the electrons induced by electrostatic induction can barely flow back and forth from the ground to the samples. Only the area between the copper wire and the composite can provide very limited paths for electron flow, resulting in low electrical outputs, as shown in Figures 2c−e and S8. In regard to the composite-based CT-TENG with a higher CB content, the electrical outputs of the pristine ones are greatly increased. This is because conductive networks are formed in the composite with increased CB content, and the electrons can flow freely throughout the composite via the metal wire. However, the outputs are still limited.

After the corona charging treatment, the electrical output performance of the charged CT-TENGs is remarkably increased. The variation trend and comparisons of the outputs are shown in Figures 2c−e and S8. The charged C-8 possesses the highest electrical outputs, including V_{OC}, I_{SC}, and Q_{SC}, while the outputs of the remaining samples display a tendency of monotonic decrease with increasing CB content in the composite. As shown in Figure 2f−h, the V_{OC}, I_{SC}, and Q_{SC} of C-8 can reach 41 V, 0.262 μA, and 14 nC, respectively. The V_{OC} is almost 8 times higher than the pristine V_{OC}. The reason why this obvious improvement is observed could be attributed to the large amount of the positive charges trapped in the CB islands, which enhance the triboelectrification effect after the corona charging process. Among these samples, C-8, with most CB islands under the percolation state, could trap most charges, thus providing the best output. When the conductive networks become denser, an increasing number of CB islands connect and form conductive networks, so the trapping sites are decreased. Thus, the charging capacity is reduced.

Generally, the work frequency is one of the factors influencing the electrical output of the TENG. To further investigate the frequency dependence, the output performance of C-8 under different frequencies was also tested. As illustrated in Figure 3a−c, when the applied frequency varied

https://doi.org/10.1021/acsami.1c13840
ACS Appl. Mater. Interfaces 2021, 13, 42966−42976

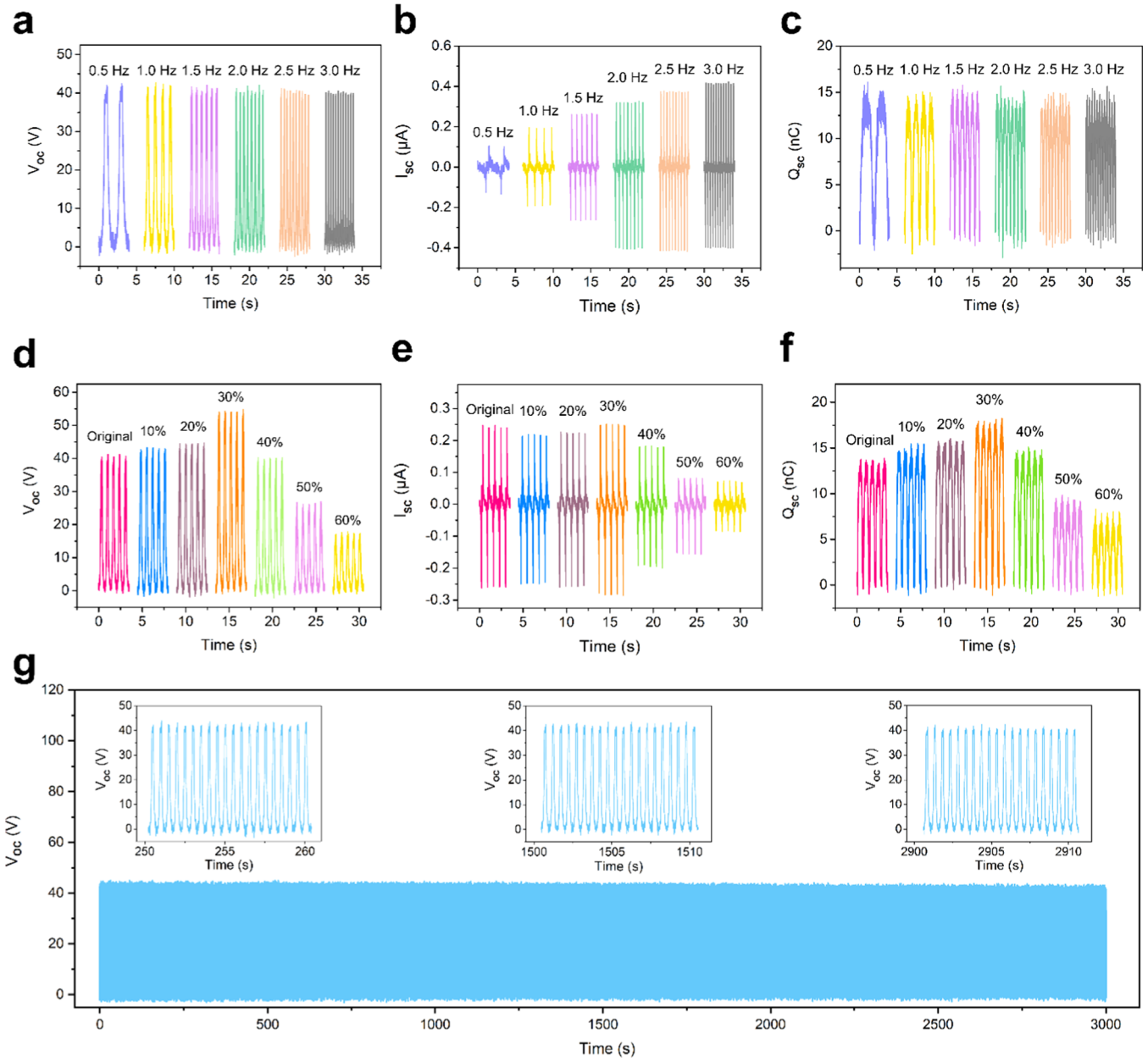

Figure 3. Electrical output and stability of the CT-TENG. (a–c) V_{OC}, I_{SC}, and Q_{SC} of the CT-TENG at different work frequencies changing from 0.5 to 3.0 Hz. (d–f) Output performance of the CT-TENG under different tensile strains. (g) Reliability and stability measurement of the CT-TENG, where the V_{OC} was recorded for 3000 s.

from 0.5 to 3.0 Hz, there were no noticeable output changes of the V_{OC} and Q_{SC}, showing almost unchanged peak values at ≈41 V and ≈14 nC, respectively. Thus, the V_{OC} and Q_{SC} of the CT-TENG are independent of the operating frequency. Meanwhile, Figure 3b shows that there is an obvious increase in I_{SC} from ≈0.126 to ≈0.417 μA with increasing operating frequency. The variation trend and comparisons of the peak values of the V_{OC}, I_{SC}, Q_{SC}, and the peak power densities at different frequencies are also summarized in Figure S9. This phenomenon occurs because the velocity of the movable friction layers increases with increasing work frequency under a fixed distance, leading to a faster electron transfer rate and a higher current output eventually.

Deformability and Durability of the CT-TENG. For stretchable single-electrode TENGs, their stretchability and their corresponding electrical output under different tensile strains are also essential requirements for their extensive applications. Thus, the relevant evaluation tests of the CT-TENG, including its mechanical performance and electrical outputs, were investigated further. The tensile strain capacity of C-8 was tested by a configurable motorized tension test stand with a digital force gauge. It showed a failure strain of 646% at 19.75 MPa (Figure S10a), which is attributed to the good stretchability of TPU and the relatively high TPU proportion in C-8. Figure S10b demonstrates that the CT-TENG was uniaxially stretched from its original length to 500%, showing good stretchability.

Because of the good stretchability of C-8, its electrical output performance under different strains was also investigated. Since the induced strain on the skin surface and joint motion does not exceed 60% strain, the range of this test is from original length to 60% strain. The electrical outputs of the

https://doi.org/10.1021/acsami.1c13840
ACS Appl. Mater. Interfaces 2021, 13, 42966–42976

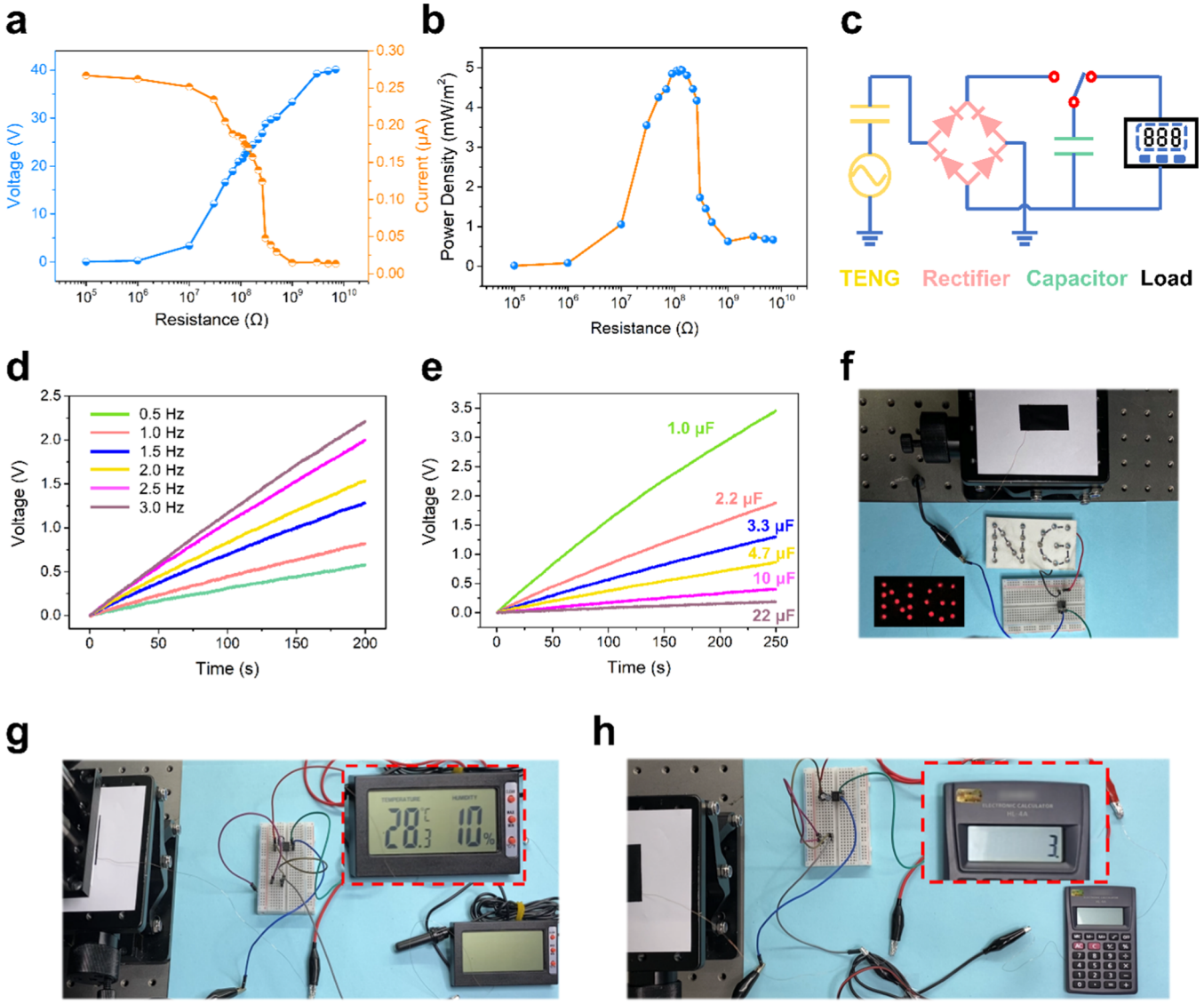

Figure 4. Demonstration of the CT-TENG for mechanical energy harvesting. (a) Dependence of the output voltage, current, and (b) power density on different external load resistances. (c) Circuit diagram for driving electronics with a rectifier and a capacitor. The charging curve of the CT-TENG at (d) different operating frequencies (0.5−3 Hz) for a 2 μF capacitor and at (e) different capacitance capacities (1−22 μF). Digital images of the CT-TENG powering (f) 20 light-emitting diodes (LEDs) patterned as "NG", (g) thermohygrometer, and (h) electronic calculator.

CT-TENG under various stretching strain levels, including the V_{OC}, I_{SC}, and Q_{SC}, slightly increased first until 30% strain (V_{OC}: 54 V, I_{SC}: 0.286 μA, Q_{SC}: 17 nC) and then decreased noticeably (Figure 3d−f). The variation trend and comparisons of the peak values of the V_{OC}, I_{SC}, and Q_{SC} and peak power densities under different tensile strains are demonstrated in Figure S11a−d. After recovering from the stretching state, the variation of V_{OC} is not obvious under the recovered state, as shown in Figure S11e. This result can be attributed to the coupling effect of the conductivity decrease and the increased contact surface area of the C-8. When the CT-TENG is stretched, the conductive networks made of CB gradually reduce the overlapping area and lose the conductive paths, thus their electrical conductivity decreases. In the early stage, only parts of the networks are affected under stretching. The conductive paths survive for electron flow and electrical output. At the same time, when the CT-TENG is stretched, the contacting surface area increases initially and then decreases.[29] With the continuous stretching of the CT-TENG, the conductive networks will be further damaged, leading to less conductive paths. A decreasing number of electrons can pass through the device, causing a further decrease in the electrical output. Thus, the initial growing stage of the output performance under strains ranging from the original state to 30% could be ascribed to the positive effects of the maintained conductivity and the increased contacting surface area under stretching. When it is further stretched to 60%, the degradation of the electrical output performance is caused by the combined negative effects of the decreased conductivity and the reduced contacting surface area.

Additionally, reliability and stability are important factors to evaluate the practicality of TENGs in practical applications. Therefore, it is essential to study abovementioned properties of CT-TENG. In Figure 3g, the V_{OC} of the C-8 remains steady, and there is no obvious deterioration observed over ~4500 repeated contact-separation cycles for 3000 s, illustrating the high reliability and stability of the CT-TENG.

https://doi.org/10.1021/acsami.1c13840
ACS Appl. Mater. Interfaces 2021, 13, 42966−42976

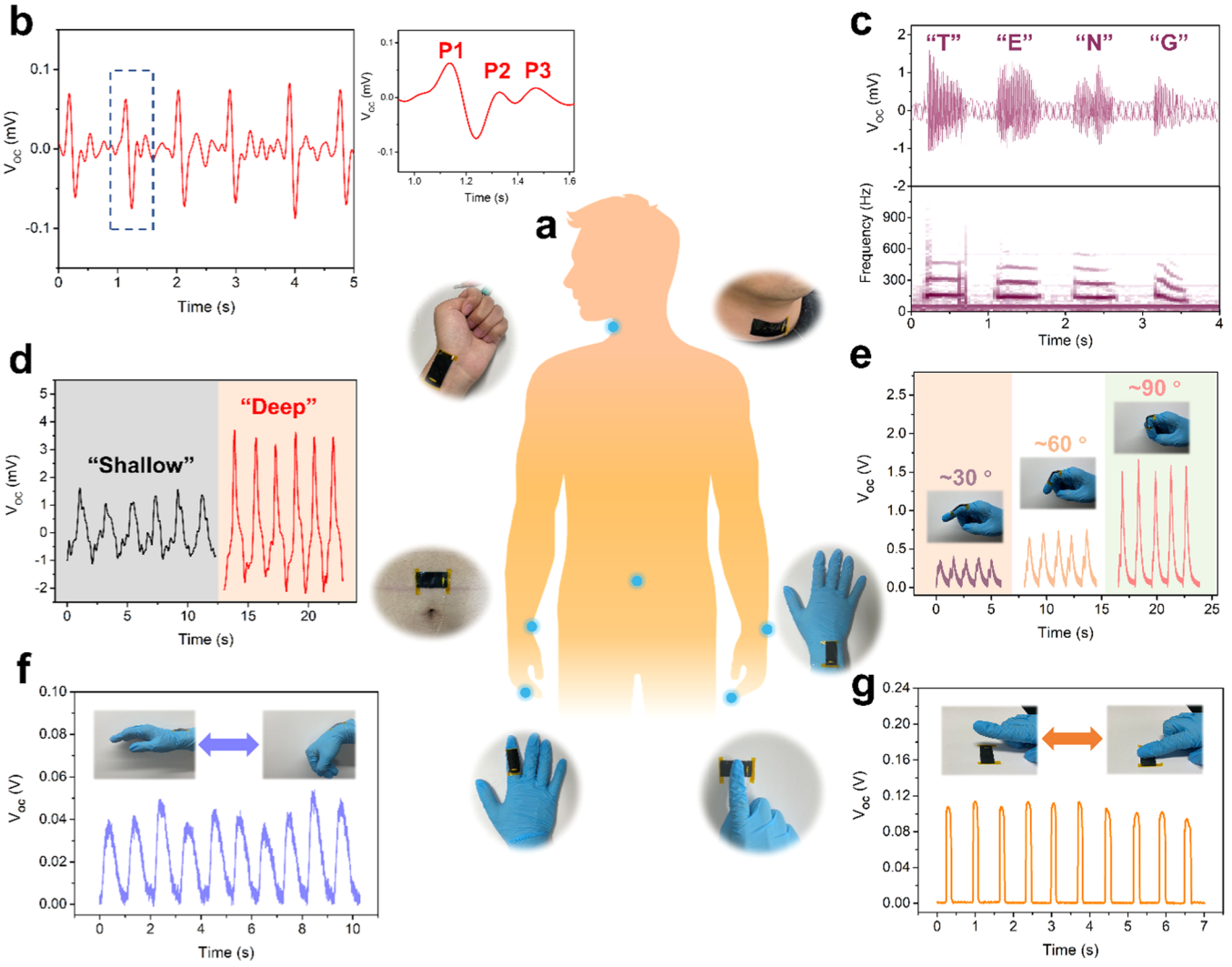

Figure 5. Physiological signals and joint movement monitoring. (a) Schematic illustration of a human body with the detected parts marked with blue solid circles. Digital images of the corresponding detected parts are also displayed. (b) Output voltage response to real-time monitoring of the radial artery pulse. The right enlarged pattern is one complete radial artery pulse waveform containing "P1," "P2," and "P3" peaks. (c) Voltage output of pronunciation of "T" "E" "N" "G" and the corresponding spectrum analysis result to detect vocal cord vibrations. (d) Abdominal respiratory monitoring by mounting the CT-TENG on the human belly. V_{OC} of the CT-TENG attached on the finger and the wrist to detect (e) finger bending, (f) wrist bending, and (g) finger tapping.

Mechanical Energy Harvesting by the CT-TENG. Since the CT-TENG possesses good electrical output performance, as shown above, it is promising to utilize the CT-TENG as a potential energy harvester. The effective power density (P) of the TENG can be calculated from the formula $P = U^2/RA$, where U is the output voltage, R is the load resistance, and A is the valid area of the TENG. To investigate the effective output performance of the C-8, we measured its output voltage and current under different external load resistances ranging from 100 kΩ to 7 GΩ. The output voltage increased with increasing external load resistance, while the current followed a downward trend according to Ohm's law, as illustrated in Figure 4a. Consequently, the instantaneous power density of the C-8 first showed an ascending tendency to a maximum power density of ~4.95 mW/m^2 at 130 MΩ and subsequently decreased (Figure 4b).

The energy generated by the CT-TENG cannot directly be used for powering direct-current (DC) electronics because it is alternating current. Therefore, the harvested electric energy should be rectified and stored in commercial capacitors or batteries for later usage instead of using it directly. To investigate the capability of the C-8 as a potential power supply, a rectifier circuit was constructed with the C-8, a bridge rectifier, a commercial capacitor, and different low-power electronic devices to form a self-charging power system, which is illustrated in Figure 4c. As shown in Figure 4d, a 2.2 μF commercial capacitor was charged at various applied frequencies (0.5−3 Hz), and the corresponding voltage variations were recorded to assess their charging capability. The charging speed progressively increases with increasing frequency. A 2.2 μF capacitor can be charged to 2 V within 178 s under an operating frequency of 3.0 Hz. Furthermore, the charging ability of the CT-TENG for different capacitors was also investigated. As demonstrated in Figure 4e, a 1 μF capacitor can be charged to 3 V within 210 s while a 2.2 μF capacitor was charged to 1.5 V in ≈193 s at 2 Hz, therefore the charging speed accelerates gradually due to capacitance reduction.

In addition, as displayed in Figure 4f and Video S1, it can be easily observed that the electricity generated by the CT-TENG

https://doi.org/10.1021/acsami.1c13840
ACS Appl. Mater. Interfaces 2021, 13, 42966−42976

can light up at least 20 LEDs patterned in the shape of the capital letters NG (which is short for a nanogenerator) instantly as we tap the CT-TENG by hand with a PTFE film. Next, the ability to power commercial electronics by the CT-TENG was also evaluated. As demonstrated in Figure 4g,h and Videos S2 and S3, sufficient energy was generated to power a thermohygrometer and an electronic calculator for mathematical operations. As shown in Figure S12, the real-time charging and discharging curve of the 47 μF capacitor for powering the calculator is also recorded. The voltage of the capacitor was charged from 0 to 1.7 V over approximately 82 min. Thus, from these demonstrations and analyses, it can be concluded that a self-powered system based on the CT-TENG could be a stable power supply for small electronics.

Applications of CT-TENG in Self-Powered Sensing. To investigate the biocompatibility of the as-prepared CT-TENG, the cytotoxicity of C-8 was evaluated by in vitro coculture with L929 cells (see the Experimental Section). As summarized in Figure S13a,b, the cells in different groups (control, C-8) after 1, 2, and 3 days of treatment showed almost the same cell viabilities, confirming the good biocompatibility of the CT-TENG. Considering its good stretchability, deformability, stability, and ability to generate different electrical signals under mechanical deformation, the CT-TENG can also be used as a biomechanical sensor for human activity monitoring. Moreover, it is convenient that the CT-TENG is a self-powered device without any need for an external power source. Therefore, the CT-TENG (C-8) can be assembled and attached to the corresponding body parts (Figure 5a) and then connected to an electrometer and an oscilloscope (Figure S14), providing a simple way for self-powered physiological signal sensing.

A pulse is one of the critical vital signs to evaluate people's physical and mental states. Here, the CT-TENG was attached to the radial artery at the wrist to measure the pulse. The real-time signals of the normal pulse and abnormal vascular occlusion events (Figures 5b and S15) were recorded by the CT-TENG, indicating good sensitivity and physiological signal sensing ability. In addition, the normal pulses displayed three obvious subtle peaks, representing radial artery pulse waveforms (P1 and P3) and systolic augmentation shoulders (P2), which exhibited a high sensing resolution.

To further demonstrate the excellent biomechanical sensing performance, the CT-TENG was attached to the throat to monitor vocal cord vibrations. A voltage signal of 1−2.5 mV was obtained when the volunteer pronounced T, E, N, and G. After short-term Fourier transform (STFT) analysis of the signal, the changes in the pronunciation of different letters could be clearly identified (Figure 5c). Normally, one complete breathing cycle can generate a rising and a falling signal caused by inhalation and exhalation, respectively. When the CT-TENG was attached to the human abdomen, the signals of the repeatable respiratory pattern were recorded. Here, shallow and deep breaths were detected and distinguished by the amplitude of the voltage signal (Figure 5d). Moreover, the CT-TENG can also be used for monitoring other human motion signals. To demonstrate the sensing capability of joint movement detection, the CT-TENG was attached on the joint of the index finger. It can be clearly seen that obvious output signals in the form of voltage are effectively detected under cyclic finger bending (Figure 5e). Furthermore, by analyzing the peak value of the output voltage, we can differentiate the bending angle of the finger. The larger the angle of finger bending, the higher the output peak voltage the CT-TENG sensor generates. The output varies from 0.45 to 1.6 V with the bending angle ranging from 30 to 90°. In addition, by attaching the CT-TENG to a wrist joint, the motions of the wrist can be successfully detected (Figure 5f). When the wrist bent back and forth, continuous voltage signals were monitored. Also, the CT-TENG can continuously sense finger tapping applied on the device, as shown in Figure 5g.

EXPERIMENTAL SECTION

Materials. TPU pellets (polyether resin, Texin 985) were supplied by Bayer AG (Bayer Material-Science, Leverkusen, Germany). CB (VULCAN XC72R) was supplied by Carbot Corporation, having a typical bulk density of 96 kg/m^3 and an average particle size of 50 nm. Tetrahydrofuran (THF) (AR, 99.0%) was purchased from Shanghai Macklin.

Fabrication of the Stretchable Composite Electrode. The fabrication procedure of the CB/TPU with different mass ratios was reported previously.[38] In brief, TPU was dissolved in THF under constant stirring at 60 °C. Next, CB was added to the TPU with different mass fractions and adequately mixed. Then, the CB/TPU mixture was poured on a substrate and wet cast by an applicator with a thickness of 1 mm. A CB/TPU film was produced until the solvent evaporated at room temperature. Subsequently, the film was cut into rectangular strips (2 × 4 cm^2) using a scalpel, and then a copper wire was attached to one side of the film as the lead wire. The corona charging process was conducted by applying a forward polarization voltage of 5 kV on the CB/TPU film for 15 min. For comparison, a pure TPU film without CB was also prepared using the same fabrication method and treated with corona charging under the same situation mentioned above.

In Vitro Cellular Viability Test (Cell Count Kit-8, CCK-8) and Cell Morphologic Immunofluorescent Staining. *Cell culture*: The L929 cell line was cultured in a 25 cm^2 flask with standard Dulbecco's modified Eagle's medium (DMEM, Gibco) supplemented with 1% penicillin/streptomycin (Gibco) and 10% fetal bovine serum (FBS, Gibco) at 37 °C in a 5% CO_2 atmosphere. *Cell viability*: The sample of CB/TPU with a weight of 100 mg was first immersed in 50 mL of DMEM for 24 h, and the leach liquor was reserved. *CCK-8 assay*: L929 cells at an initial density of 1 × 106 cells/well in the log phase of growth in 1 mL of leach liquor of CB/TPU were seeded in 24-well plates. Wells with 1 mL of standard DMEM were used as the control group. The cells were cultured and stimulated for 1, 2, and 3 days, and the cell proliferation level was evaluated by a Cell Count Kit-8 (CCK-8, Dojindo Molecular Technologies, Inc., Japan). After removing the culture medium and washing the cells with a phosphate-buffered saline solution (PBS), 210 μL of a complete medium including 10 μL of a CCK-8 reagent was added. After incubation for 2 h, 150 μL of the culture supernatant was transferred to a 96-well plate, and the absorbance was measured at 450 nm. Each group had five parallel wells. *Cell morphology and immunofluorescent staining*: To visualize the cytoskeleton, F-actin (green) was stained with phalloidin. Before staining, the cells were washed with PBS three times. Then, the cells were fixed for 10 min and stained with phalloidin for 40 min at room temperature. The stained cells were visualized by laser scanning confocal microscopy (Leica SP8).

CHARACTERIZATION AND MEASUREMENT

The voltage for corona charging was applied via a high-voltage polarization instrument (Nanjing Entai Electronic Instruments ET 2673A). Fourier transform infrared (FT-IR) spectra were recorded on a VERTEX80v spectrometer (Bruker, Karlsruhe, Germany) using the attenuated total reflectance (ATR) technique. All of the spectra were scanned in the range from 500 to 4000 cm^{-1}. The morphologies of the samples were obtained using a field-emission scanning electron microscope (FESEM, NOVA 450). A linear motor (LinMot E1100) was

https://doi.org/10.1021/acsami.1c13840
ACS Appl. Mater. Interfaces 2021, 13, 42966−42976

applied to provide periodic contact-separation movement for the CT-TENG electrical measurements. By varying the velocity of the linear motor at a fixed step distance, the CT-TENG could work under different frequencies. The V_{OC}, I_{SC}, and Q_{SC} of the CT-TENG were measured by a Keithley 6517 electrometer and were recorded by an oscilloscope (LeCroy HDO6104). In the physiological signal sensing measurements, pulse, vocal cord vibration, and breath sensing were directly recorded using an oscilloscope and finger bending, tapping, and wrist bending sensing were detected using an electrometer.

CONCLUSIONS

In summary, based on this CB/TPU composite, we have developed a stretchable, ultrathin, and chargeable CT-TENG that can harvest mechanical energy to power commercial electronics and realize physiological signal sensing. The CT-TENG can achieve a strain of approximately 646% and the total thickness is only 50 μm. The CB/TPU composite works not only as an electrode but also as a triboelectrification layer. Using the corona charging approach, the CT-TENG with an effective area of 2 × 4 cm^2 produces a V_{OC} of 41 V in a single-electrode mode. The output performance is remarkably improved after charging treatment, and the V_{OC} is 8 times higher than that of the pristine device. This is the first time that a triboelectric electrode material has been improved by postcharging treatment. Additionally, the CT-TENG can work as a sustainable power source for commercial electronics by harvesting mechanical energy. In particular, based on the advantages of the CT-TENG, it can be used as a biomechanical sensor to monitor the radial artery pulse, sounds, abdominal respiration, and different real-time human motions. Hence, the proposed CT-TENG has great potential as a self-powered sensory system or as an energy supplier for next-generation wearable electronics and other fields in the future.

ASSOCIATED CONTENT

Supporting Information

The Supporting Information is available free of charge at https://pubs.acs.org/doi/10.1021/acsami.1c13840.

SEM images of the CB/TPU composites (Figure S1), electrical conductivity of different CB/TPU composites (Figure S2), image of a large-scale fabricated C-8 composite film (Figure S3), thickness and weight of the fabricated CT-TENG (Figure S4), FT-IR analysis of all of the CB/TPU composites (Figure S5), schematic diagram of the detailed change of the CT-TENG during the corona charging process (Figure S6), simulation of electrical potential distributions of the CT-TENG (Figure S7), variation trend and comparisons of outputs of all of the prepared CT-TENGs before and after corona charging (Figure S8), relationship between different frequencies and corresponding outputs (Figure S9), stretchability tests of the CT-TENG (Figure S10), relationship between different tensile strains and corresponding outputs (Figure S11), charging and discharging curves of a capacitor connected with a calculator (Figure S12), characterization of biocompatibility of the C-8 (Figure S13), physiological signals sensing setup of the CT-TENG and the measurement equipment (Figure S14), and signals of normal pulse and abnormal vascular occlusion event (Figure S15) (PDF)

Video S1 (MP4)

Video S2 (MP4)

Video S3-revised-r2 (MP4)

AUTHOR INFORMATION

Corresponding Authors

Han Ouyang − *School of Nanoscience and Technology, University of Chinese Academy of Sciences, Beijing 100049, People's Republic of China; Key Laboratory for Biomechanics and Mechanobiology of Chinese Education Ministry, Beijing Advanced Innovation Centre for Biomedical Engineering, School of Biological Science and Medical Engineering, Beihang University, Beijing 100083, People's Republic of China*; Email: ouyanghan@buaa.edu.cn

Zhou Li − *CAS Center for Excellence in Nanoscience, Beijing Key Laboratory of Micro-Nano Energy and Sensor, Beijing Institute of Nanoenergy and Nanosystems, Chinese Academy of Sciences, Beijing 101400, People's Republic of China; School of Nanoscience and Technology, University of Chinese Academy of Sciences, Beijing 100049, People's Republic of China; Center on Nanoenergy Research School of Physical Science and Technology, Guangxi University, Nanning 530004, People's Republic of China*; orcid.org/0000-0002-9952-7296; Email: zli@binn.cas.cn

Authors

Weiyi Zhang − *School of Microelectronics, Tianjin University, Tianjin 300072, People's Republic of China; CAS Center for Excellence in Nanoscience, Beijing Key Laboratory of Micro-Nano Energy and Sensor, Beijing Institute of Nanoenergy and Nanosystems, Chinese Academy of Sciences, Beijing 101400, People's Republic of China*

Qiang Liu − *School of Microelectronics, Tianjin University, Tianjin 300072, People's Republic of China*

Shengyu Chao − *CAS Center for Excellence in Nanoscience, Beijing Key Laboratory of Micro-Nano Energy and Sensor, Beijing Institute of Nanoenergy and Nanosystems, Chinese Academy of Sciences, Beijing 101400, People's Republic of China; School of Nanoscience and Technology, University of Chinese Academy of Sciences, Beijing 100049, People's Republic of China*

Ruping Liu − *Beijing Institute of Graphic Communication, Beijing 102600, People's Republic of China*

Xi Cui − *CAS Center for Excellence in Nanoscience, Beijing Key Laboratory of Micro-Nano Energy and Sensor, Beijing Institute of Nanoenergy and Nanosystems, Chinese Academy of Sciences, Beijing 101400, People's Republic of China; School of Nanoscience and Technology, University of Chinese Academy of Sciences, Beijing 100049, People's Republic of China*

Yu Sun − *CAS Center for Excellence in Nanoscience, Beijing Key Laboratory of Micro-Nano Energy and Sensor, Beijing Institute of Nanoenergy and Nanosystems, Chinese Academy of Sciences, Beijing 101400, People's Republic of China*

Complete contact information is available at: https://pubs.acs.org/10.1021/acsami.1c13840

Author Contributions

Z.L. and H.O. supervised the project. W.Z., Q.L., R.L., and H.O. conceived the idea and designed the experiments. W.Z. and Y.S. fabricated the devices and performed the characterizations, except for those mentioned below. W.Z. accomplished

the material characterization. X.C., R.L., and Y.S. carried out the in vitro cellular viability test. W.Z., H.O., and Z.L. wrote the manuscript, and all authors reviewed and commented on the manuscript.

Notes

The authors declare no competing financial interest.

■ ACKNOWLEDGMENTS

The authors thank the National Natural Science Foundation of China (61875015, 62004010, 61971049), the Beijing Natural Science Foundation (JQ20038), the Key Scientific Research Project of Beijing Municipal Commission of Education (kz202010015024), the Research and Development Program of BIGC (Ec202006), and The Fundamental Research Funds for the Central Universities for their support.

■ REFERENCES

(1) Chung, H. U.; Kim, B. H.; Lee, J. Y.; Lee, J.; Xie, Z.; Ibler, E. M.; Lee, K.; Banks, A.; Jeong, J. Y.; Kim, J.; Ogle, C.; Grande, D.; Yu, Y.; Jang, H.; Assem, P.; Ryu, D.; Kwak, J. W.; Namkoong, M.; Park, J. B.; Lee, Y.; Kim, D. H.; Ryu, A.; Jeong, J.; You, K.; Ji, B.; Liu, Z.; Huo, Q.; Feng, X.; Deng, Y.; Xu, Y.; Jang, K.-I.; Kim, J.; Zhang, Y.; Ghaffari, R.; Rand, C. M.; Schau, M.; Hamvas, A.; Weese-Mayer, D. E.; Huang, Y.; Lee, S. M.; Lee, C. H.; Shanbhag, N. R.; Paller, A. S.; Xu, S.; Rogers, J. A. Binodal, Wireless Epidermal Electronic Systems with In-Sensor Analytics for Neonatal Intensive Care. *Science* **2019**, *363*, No. eaau0780.

(2) Dong, K.; Peng, X.; Wang, Z. L. Fiber/Fabric-Based Piezoelectric and Triboelectric Nanogenerators for Flexible/Stretchable and Wearable Electronics and Artificial Intelligence. *Adv. Mater.* **2020**, *32*, No. 1902549.

(3) Peng, X.; Dong, K.; Ye, C.; Jiang, Y.; Zhai, S.; Cheng, R.; Liu, D.; Gao, X.; Wang, J.; Wang, Z. L. A Breathable, Biodegradable, Antibacterial, and Self-Powered Electronic Skin Based on All-Nanofiber Triboelectric Nanogenerators. *Sci Adv.* **2020**, *6*, No. eaba9624.

(4) Choi, S.; Lee, H.; Ghaffari, R.; Hyeon, T.; Kim, D.-H. Recent Advances in Flexible and Stretchable Bio-Electronic Devices Integrated with Nanomaterials. *Adv. Mater.* **2016**, *28*, 4203−4218.

(5) Lee, J.; Zambrano, B. L.; Woo, J.; Yoon, K.; Lee, T. Recent Advances in 1D Stretchable Electrodes and Devices for Textile and Wearable Electronics: Materials, Fabrications, and Applications. *Adv. Mater.* **2020**, *32*, No. 1902532.

(6) Dong, K.; Wu, Z.; Deng, J.; Wang, A. C.; Zou, H.; Chen, C.; Hu, D.; Gu, B.; Sun, B.; Wang, Z. L. A Stretchable Yarn Embedded Triboelectric Nanogenerator as Electronic Skin for Biomechanical Energy Harvesting and Multifunctional Pressure Sensing. *Adv. Mater.* **2018**, *30*, No. 1804944.

(7) Kim, C.-C.; Lee, H.-H.; Oh, K. H.; Sun, J.-Y. Highly Stretchable, Transparent Ionic Touch Panel. *Science* **2016**, *353*, 682−687.

(8) Son, D.; Kang, J.; Vardoulis, O.; Kim, Y.; Matsuhisa, N.; Oh, J. Y.; To, J. W. F.; Mun, J.; Katsumata, T.; Liu, Y.; McGuire, A. F.; Krason, M.; Molina-Lopez, F.; Ham, J.; Kraft, U.; Lee, Y.; Yun, Y.; Tok, J. B. H.; Bao, Z. An Integrated Self-Healable Electronic Skin System Fabricated via Dynamic Reconstruction of A Nanostructured Conducting Network. *Nat. Nanotechnol.* **2018**, *13*, 1057−1065.

(9) He, T.; Wang, H.; Wang, J.; Tian, X.; Wen, F.; Shi, Q.; Ho, J. S.; Lee, C. Self-Sustainable Wearable Textile Nano-Energy Nano-System (NENS) for Next-Generation Healthcare Applications. *Adv. Sci.* **2019**, *6*, No. 1901437.

(10) Yu, Y.; Zhai, Y.; Yun, Z.; Zhai, W.; Wang, X.; Zheng, G.; Yan, C.; Dai, K.; Liu, C.; Shen, C. Ultra-Stretchable Porous Fiber-Shaped Strain Sensor with Exponential Response in Full Sensing Range and Excellent Anti-Interference Ability Toward Buckling, Torsion, Temperature, and Humidity. *Adv. Electron Mater.* **2019**, *5*, No. 1900538.

(11) Zhai, Y.; Yu, Y.; Zhou, K.; Yun, Z.; Huang, W.; Liu, H.; Xia, Q.; Dai, K.; Zheng, G.; Liu, C.; Shen, C. Flexible and Wearable Carbon Black/Thermoplastic Polyurethane Foam with A Pinnate-Veined Aligned Porous Structure for Multifunctional Piezoresistive Sensors. *Chem. Eng. J.* **2020**, *382*, No. 122985.

(12) Liu, W.; Wang, Z.; Wang, G.; Liu, G.; Chen, J.; Pu, X.; Xi, Y.; Wang, X.; Guo, H.; Hu, C.; Wang, Z. L. Integrated Charge Excitation Triboelectric Nanogenerator. *Nat. Commun.* **2019**, *10*, No. 1426.

(13) Li, T.; Zou, J.; Xing, F.; Zhang, M.; Cao, X.; Wang, N.; Wang, Z. L. From Dual-Mode Triboelectric Nanogenerator to Smart Tactile Sensor: A Multiplexing Design. *ACS Nano* **2017**, *11*, 3950−3956.

(14) Liu, D.; Yin, X.; Guo, H.; Zhou, L.; Li, X.; Zhang, C.; Wang, J.; Wang, Z. L. A Constant Current Triboelectric Nanogenerator Arising from Electrostatic Breakdown. *Sci. Adv.* **2019**, *5*, No. eaav6437.

(15) Wang, L.; Wang, L.; Zhang, Y.; Pan, J.; Li, S.; Sun, X.; Zhang, B.; Peng, H. Weaving Sensing Fibers into Electrochemical Fabric for Real-Time Health Monitoring. *Adv. Funct. Mater.* **2018**, *28*, No. 1804456.

(16) Chen, X.; Wu, Y.; Shao, J.; Jiang, T.; Yu, A.; Xu, L.; Wang, Z. L. On-Skin Triboelectric Nanogenerator and Self-Powered Sensor with Ultrathin Thickness and High Stretchability. *Small* **2017**, *13*, No. 1702929.

(17) Yang, Y.; Sun, N.; Wen, Z.; Cheng, P.; Zheng, H.; Shao, H.; Xia, Y.; Chen, C.; Lan, H.; Xie, X.; Zhou, C.; Zhong, J.; Sun, X.; Lee, S.-T. Liquid-Metal-Based Super-Stretchable and Structure-Designable Triboelectric Nanogenerator for Wearable Electronics. *ACS Nano* **2018**, *12*, 2027−2034.

(18) Lim, H.-R.; Kim, H. S.; Qazi, R.; Kwon, Y.-T.; Jeong, J.-W.; Yeo, W.-H. Advanced Soft Materials, Sensor Integrations, and Applications of Wearable Flexible Hybrid Electronics in Healthcare, Energy, and Environment. *Adv. Mater.* **2020**, *32*, No. 1901924.

(19) Wang, L.; Liu, W.; Yan, Z.; Wang, F.; Wang, X. Stretchable and Shape-Adaptable Triboelectric Nanogenerator Based on Biocompatible Liquid Electrolyte for Biomechanical Energy Harvesting and Wearable Human-Machine Interaction. *Adv. Funct. Mater.* **2021**, *31*, No. 2007221.

(20) Luo, J.; Wang, Z.; Xu, L.; Wang, A. C.; Han, K.; Jiang, T.; Lai, Q.; Bai, Y.; Tang, W.; Fan, F. R.; Wang, Z. L. Flexible and Durable Wood-Based Triboelectric Nanogenerators for Self-Powered Sensing in Athletic Big Data Analytics. *Nat. Commun.* **2019**, *10*, No. 5147.

(21) Liu, Y.; Liu, W.; Wang, Z.; He, W.; Tang, Q.; Xi, Y.; Wang, X.; Guo, H.; Hu, C. Quantifying Contact Status and The Air-Breakdown Model of Charge-Excitation Triboelectric Nanogenerators to Maximize Charge Density. *Nat. Commun.* **2020**, *11*, No. 1599.

(22) Liu, W.; Wang, Z.; Wang, G.; Zeng, Q.; He, W.; Liu, L.; Wang, X.; Xi, Y.; Guo, H.; Hu, C.; Wang, Z. L. Switched-Capacitor-Convertors Based on Fractal Design for Output Power Management of Triboelectric Nanogenerator. *Nat. Commun.* **2020**, *11*, No. 1883.

(23) Liang, X.; Jiang, T.; Liu, G.; Xiao, T.; Xu, L.; Li, W.; Xi, F.; Zhang, C.; Wang, Z.L. Triboelectric Nanogenerator Networks Integrated with Power Management Module for Water Wave Energy Harvesting. *Adv. Funct. Mater.* **2019**, *29*, No. 1807241.

(24) Li, X.; Yin, X.; Zhao, Z.; Zhou, L.; Liu, D.; Zhang, C.; Zhang, C.; Zhang, W.; Li, S.; Wang, J.; Wang, Z. L. Long-Lifetime Triboelectric Nanogenerator Operated in Conjunction Modes and Low Crest Factor. *Adv. Energy Mater.* **2020**, *10*, No. 1903024.

(25) Dong, K.; Peng, X.; An, J.; Wang, A. C.; Luo, J.; Sun, B.; Wang, J.; Wang, Z. L. Shape Adaptable and Highly Resilient 3D Braided Triboelectric Nanogenerators as E-Textiles for Power and Sensing. *Nat. Commun.* **2020**, *11*, No. 2868.

(26) Jiang, Y.; Dong, K.; Li, X.; An, J.; Wu, D.; Peng, X.; Yi, J.; Ning, C.; Cheng, R.; Yu, P.; Wang, Z. L. Stretchable, Washable, and Ultrathin Triboelectric Nanogenerators as Skin-Like Highly Sensitive Self-Powered Haptic Sensors. *Adv. Funct. Mater.* **2021**, *31*, No. 2005584.

(27) Lai, Y.-C.; Wu, H.-M.; Lin, H.-C.; Chang, C.-L.; Chou, H.-H.; Hsiao, Y.-C.; Wu, Y.-C. Entirely, Intrinsically, and Autonomously Self-healable, Highly Transparent, and Superstretchable Triboelectric

https://doi.org/10.1021/acsami.1c13840
ACS Appl. Mater. Interfaces 2021, 13, 42966−42976

Nanogenerator for Personal Power Sources and Self-Powered Electronic Skins. *Adv. Funct. Mater.* **2019**, *29*, No. 1904626.
(28) Zhao, X.; Zhang, D.; Xu, S.; Qian, W.; Han, W.; Wang, Z. L.; Yang, Y. Stretching-Enhanced Triboelectric Nanogenerator for Efficient Wind Energy Scavenging and Ultrasensitive Strain Sensing. *Nano Energy* **2020**, *75*, No. 104920.
(29) Cao, W.-T.; Ouyang, H.; Xin, W.; Chao, S.; Ma, C.; Li, Z.; Chen, F.; Ma, M.-G. A Stretchable Highoutput Triboelectric Nanogenerator Improved by MXene Liquid Electrode with High Electronegativity. *Adv. Funct. Mater.* **2020**, *30*, No. 2004181.
(30) Li, S.; Wang, J.; Peng, W.; Lin, L.; Zi, Y.; Wang, S.; Zhang, G.; Wang, Z. L. Sustainable Energy Source for Wearable Electronics Based on Multilayer Elastomeric Triboelectric Nanogenerators. *Adv. Energy Mater.* **2017**, *7*, No. 1602832.
(31) Fan, Y. J.; Meng, X. S.; Li, H. Y.; Kuang, S. Y.; Zhang, L.; Wu, Y.; Wang, Z. L.; Zhu, G. Stretchable Porous Carbon Nanotube-Elastomer Hybrid Nanocomposite for Harvesting Mechanical Energy. *Adv. Mater.* **2017**, *29*, No. 1603115.
(32) Parida, K.; Kumar, V.; Wang, J.; Bhavanasi, V.; Bendi, R.; Lee, P. S. Highly Transparent, Stretchable, and Self-Healing Ionic-Skin Triboelectric Nanogenerators for Energy Harvesting and Touch Applications. *Adv. Mater.* **2017**, *29*, No. 1702181.
(33) Zhao, G.; Zhang, Y.; Shi, N.; Liu, Z.; Zhang, X.; Wu, M.; Pan, C.; Liu, H.; Li, L.; Wang, Z. L. Transparent and Stretchable Triboelectric Nanogenerator for Self-Powered Tactile Sensing. *Nano Energy* **2019**, *59*, 302−310.
(34) Kwak, S. S.; Kim, H.; Seung, W.; Kim, J.; Hinchet, R.; Kim, S.-W. Fully Stretchable Textile Triboelectric Nanogenerator with Knitted Fabric Structures. *ACS Nano* **2017**, *11*, 10733−10741.
(35) Cheon, S.; Kang, H.; Kim, H.; Son, Y.; Lee, J. Y.; Shin, H.-J.; Kim, S.-W.; Cho, J. H. High-Performance Triboelectric Nanogenerators Based on Electrospun Polyvinylidene Fluoride-Silver Nanowire Composite Nanofibers. *Adv. Funct. Mater.* **2018**, *28*, No. 1703778.
(36) Xia, X.; Chen, J.; Liu, G.; Javed, M. S.; Wang, X.; Hu, C. Aligning Graphene Sheets in PDMS for Improving Output Performance of Triboelectric Nanogenerator. *Carbon* **2017**, *111*, 569−576.
(37) Yang, Y.; Han, J.; Huang, J.; Sun, J.; Wang, Z. L.; Seo, S.; Sun, Q. Stretchable Energy-Harvesting Tactile Interactive Interface with Liquid-Metal-Nanoparticle-Based Electrodes. *Adv. Funct. Mater.* **2020**, *30*, No. 1909652.
(38) Zhang, W.; Liu, Q.; Chen, P. Flexible Strain Sensor Based on Carbon Black/Silver Nanoparticles Composite for Human Motion Detection. *Materials* **2018**, *11*, No. 1836.
(39) Choi, J. H.; Ra, Y.; Cho, S.; La, M.; Park, S. J.; Choi, D. Electrical Charge Storage Effect in Carbon Based Polymer Composite for Long-Term Performance Enhancement of The Triboelectric Nanogenerator. *Compos. Sci. Technol.* **2021**, *207*, No. 108680.
(40) Zheng, Y.; Li, Y.; Dai, K.; Liu, M.; Zhou, K.; Zheng, G.; Liu, C.; Shen, C. Conductive Thermoplastic Polyurethane Composites with Tunable Piezoresistivity by Modulating The Filler Dimensionality for Flexible Strain Sensors. *Composites, Part A* **2017**, *101*, 41−49.
(41) Li, H.; Guo, Z.; Kuang, S.; Wang, H.; Wang, Y.; Wu, T.; Wang, Z. L.; Zhu, G. Nanocomposite Electret with Surface Potential Self-Recovery from Water Dipping for Environmentally Stable Energy Harvesting. *Nano Energy* **2019**, *64*, No. 103913.
(42) Shao, J. J.; Tang, W.; Jiang, T.; Chen, X. Y.; Xu, L.; Chen, B. D.; Zhou, T.; Deng, C. R.; Wang, Z. L. A Multi-Dielectric-Layered Triboelectric Nanogenerator as Energized by Corona Discharge. *Nanoscale* **2017**, *9*, 9668−9675.
(43) Zheng, Y.; Li, Y.; Dai, K.; Wang, Y.; Zheng, G.; Liu, C.; Shen, C. A Highly Stretchable and Stable Strain Sensor Based on Hybrid Carbon Nanofillers/Polydimethylsiloxane Conductive Composites for Large Human Motions Monitoring. *Compos. Sci. Technol.* **2018**, *156*, 276−286.
(44) Zhang, Q.; Wang, J.; Yu, J.; Guo, Z.-X. Improved Electrical Conductivity of TPU/Carbon Black Composites by Addition of COPA and Selective Localization of Carbon Black at The Interface of Sea-Island Structured Polymer Blends. *Soft Matter* **2017**, *13*, 3431−3439.

https://doi.org/10.1021/acsami.1c13840
ACS Appl. Mater. Interfaces 2021, 13, 42966−42976